J Mater Sci (2008) 43:1539–1545
DOI 10.1007/s10853-007-2348-5

Age-hardening behaviour of a spinodally decomposed low-carat gold alloy

Mi-Gyoung Park · Chin-Ho Yu · Hyo-Joung Seol · Yong Hoon Kwon · Hyung-Il Kim

Received: 18 July 2007 / Accepted: 27 November 2007 / Published online: 1 January 2008

Abstract The age-hardening behaviour of a spinodally decomposed low-carat gold alloy was investigated by means of hardness test, X-ray diffraction (XRD), field emission scanning electron microscopic (FESEM) observations, and energy dispersive spectrometer (EDS). An apparent hardness increase occurred at the initial stage of the aging process without incubation periods. Then, after a plateau, the hardness increased to the maximum value, and finally, the softening by overaging occurred. The age-hardening of the specimen is characterized by the fast increasing rate in hardness and the apparent delay of softening. By aging the solution-treated specimen, the fcc α_0 phase was transformed into the Ag-rich α_1, Cu-rich α_2, and Zn–Pd-rich β phases through the spinodal decomposition process and the metastable phase formation. The first hardening stage which occurred during the early stage of spinodal decomposition without an apparent structural change was thought to be due to the interaction of dislocation with solute-rich fluctuations. The second hardening stage after the plateau was caused by the formation of the fine block-like structure with high coherency induced by the spinodal decomposition, which corresponded to the phase transformation of the metastable Ag-rich α_1' phase into the stable Ag-rich α_1 phase. The remarkably delayed softening was caused by the slow progress of coarsening and resultant chaining of the Ag-rich α_1 precipitates in the Cu-rich α_2 matrix due to the uniform fine scale of the structure.

M.-G. Park · C.-H. Yu · H.-J. Seol · Y. H. Kwon · H.-I. Kim (✉)
Department of Dental Materials, School of Dentistry and Medical Research Institute, Pusan National University, 1-10 Ami-dong, Seo-gu, Pusan 602-739, South Korea
e-mail: hilkim@pusan.ac.kr

Introduction

Dental gold alloys have been used for dental restorative materials because they have useful characteristics such as longevity, easy workability, biocompatibility, and maximum range of indications. Conventional dental gold alloys are ternary alloys of gold, silver, and copper with small amounts of other elements and should contain gold and platinum group metals of more than 75 wt% for chemical stability in the oral environment [1]. However, the gold price climb demanded alternative dental alloys, and this resulted in numerous low-carat gold alloys which have reduced gold content but satisfy required mechanical properties being introduced in the market. The low-carat gold alloys basically consist of gold, silver, and copper and can be hardened by an appropriate heat treatment. The hardening mechanisms of the ternary Au–Ag–Cu alloys have been reported to be due to phase transformations such as ordering, precipitation, and spinodal decomposition depending on the alloy composition and the aging temperature [2–10].

Although the interest of the low-carat gold alloys has been increased, the hardening mechanisms of these alloys have not been completely elucidated because of their complex combinations of constituents. In the present study, the age-hardening behaviour of a spinodally decomposed low-carat gold alloy was investigated. The purpose of the present study is to clarify the age-hardening mechanism by elucidating the hardness changes, phase transformation and changes in the microstructure and element distribution during the aging process.

Materials and methods

The alloy used in the present study was a commercial dental gold alloy of nominal composition 55.0 wt%

Au–19.9 wt% Ag–17.0 wt% Cu–4.0 wt% Zn–3.0 wt% Pd–1.0 wt% Pt–0.1 wt% Ir as listed in Table 1 (Goldenian C-55, Shinhung, Korea). This specimen alloy of a plate-like shape is supplied in a rolled and annealed state.

Before hardness test, the above-mentioned plate-like specimens were solution-treated at 750 °C for 10 min under an argon atmosphere and then rapidly quenched into ice brine to prevent transformation. After that, they were isothermally aged at 350, 400, and 450 °C for various periods of time in a molten salt bath (25% KNO_3 + 30% KNO_2 + 25% $NaNO_3$ + 20% $NaNO_2$) which was used for the temperature range of 150–550 °C, then quenched into ice brine for hardness test.

Hardness measurements were made using a Vickers micro-hardness tester (MVK-H1, Akashi Co., Japan) with a load of 300 gf and dwell time of 10 s. Vickers hardness results were obtained as the average values of five measurements.

For the XRD study, powder specimens which passed through a 330-mesh screen were obtained by filing the plate-like samples. After being vacuum-sealed in a silica tube and solution-treated at 750 °C for 10 min, they were isothermally aged at 350, 400, and 450 °C for various periods of time in a molten salt bath and then quenched into ice brine. The XRD profiles were recorded by an X-ray diffractometer which was operated at 30 kV and 40 mA, and Nickel-filtered Cu Kα radiation was used as the incident beam.

For the FESEM observations, plate-like samples were subjected to the required heat treatment, and then they were prepared by utilizing a standard metallographic technique. A freshly prepared aqueous solution of 10% potassium cyanide and 10% ammonium persulfate was utilized for the final etching of the samples. The specimens were examined at 15 kV using a field emission scanning electron microscope (JSM-6700F, JEOL, Japan)

EDS was done to observe the distributional changes of each element in the specimen alloy during the aging process. An energy dispersive X-Ray spectrometer (INCA x-sight, Oxford Instruments Ltd., UK) of field emission scanning electron microscope (JSM-6700F, JEOL, Japan) was used at 15 kV to examine the plate-like specimens which were used for the FESEM observations.

Table 1 Chemical composition of the alloy used

Composition	Au	Ag	Cu	Zn	Pd	Pt	Ir
wt%	55.0	19.9	17.0	4.0	3.0	1.0	0.1
at%	33.8	22.3	32.4	7.4	3.4	0.63	0.07

Results and discussion

Hardness changes

To investigate the age-hardening behaviour of the specimen alloy, the isothermal age-hardening curves were obtained at 350, 400, and 450 °C. Figure 1 shows the age-hardening curves of the specimen alloy aged isothermally at 350, 400, and 450 °C. The age-hardening behaviour of the specimen alloy aged in these temperature ranges showed a similar tendency. An apparent hardness increase occurred at an initial stage of the aging process without incubation periods. Then, after showing a plateau, the hardness increased again to the maximum value. Finally, the decrease in hardness by overaging occurred.

In Fig. 1, the maximum hardness value was lower and was obtained within shorter aging time at higher aging temperature due to the faster diffusion. The age-hardening of this alloy is characterized by the fast increasing rate in hardness and the apparent delay of softening. From the similarity in the age-hardening behaviours at 350, 400, and 450 °C, the age-hardening at these temperature ranges was supposed to undergo the same mechanism.

Phase transformation

Variations of XRD pattern during the isothermal aging were examined to clarify the age-hardening mechanism of the specimen alloy. Figure 2 shows XRD changes during the isothermal aging at 400 °C with aging time. The XRD

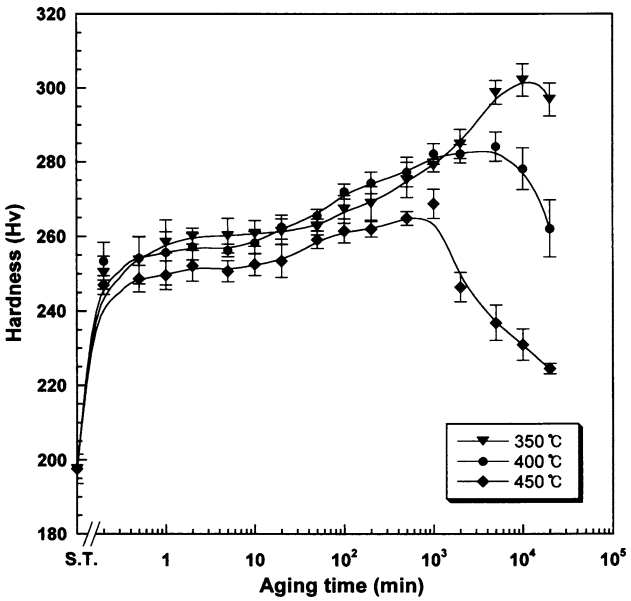

Fig. 1 Isothermal age-hardening curves of the specimen aged at 350, 400, and 450 °C

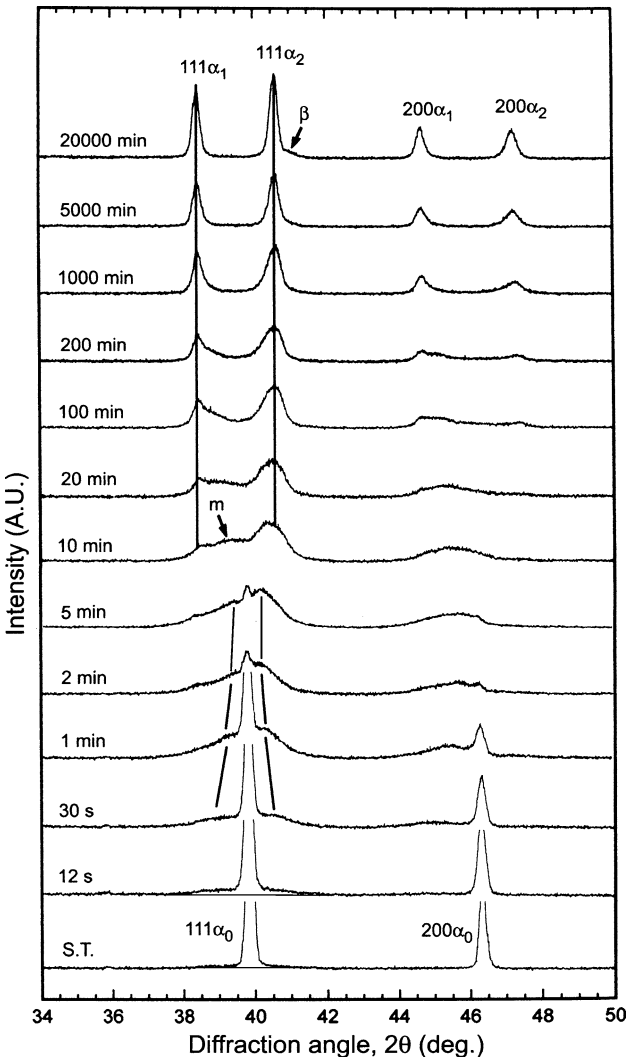

Fig. 2 Variations of XRD pattern during the isothermal aging at 400 °C with aging time

pattern of the solution-treated specimen at 750 °C for 10 min shows a single phase, α_0 of a face-centered cubic (fcc) structure with a lattice parameter of $a_{200} = 3.915$ Å. By aging the solution-treated specimen at 400 °C for 20,000 min, the α_0 phase was transformed into the fcc α_1 and α_2 phases of strong peak intensity and the β phase of very weak peak intensity. The lattice parameter of the α_1 and α_2 phases was $a_{200} = 4.054$ Å and $a_{200} = 3.846$ Å, respectively. The main components, Au, Ag, and Cu in the specimen alloy have a fcc structure with a lattice parameter of $a = 4.0786$ Å, $a = 4.0863$ Å and $a = 3.6148$ Å, respectively [11]. Considering the fact that Au is soluble with Ag and Cu at any atomic ratio, but Ag and Cu has solubility limit for each other [12], it was thought that the single α_0 phase was separated into the Au-containing two phases of Ag-rich (α_1) and Cu-rich (α_2). As both the Ag-rich α_1 and Cu-rich α_2 phases contained Au and small amounts of other ingredients, their lattice parameter was a little different from that of the pure Ag and Cu, respectively. The lattice parameter of the β phase was not clear because its diffraction peak had a very weak intensity and overlapped with the 111 peak of the α_2 phase. However, from the EDS result, the β phase was identified as the Zn–Pd-rich phase, as it will be revealed in EDS analysis. Even though a final change in the XRD pattern during the isothermal aging at 400 °C was the formation of the stable α_1, α_2, and β phases from the single α_0 phase, the spinodal decomposition of the parent α_0 phase and the metastable phase formation were observed before the stable phases formation.

To understand the relation between the hardness changes and the phase transformation, the changes in XRD pattern (Fig. 2) were compared with the changes in hardness at 400 °C (Fig. 1). In Fig. 1, the hardness increased apparently within 12 s, and then showed the plateau stage until the aging time between 5 min and 10 min. The XRD pattern at the aging time of 12 s did not show an apparent change except for an appearance of weak and wide side bands in both sides of the 111 α_0 peak, as can be seen by comparing the background line for the 111 α_0 peak at 12 s with that at the solution-treated state (S.T.). After the aging time of 12 s, the spinodal decomposition of the parent α_0 phase progressed apparently. That is, the side bands became apparent and moved closer to the 111 α_0 peak as the intensity of the 111 α_0 peak decreased with aging time, and finally the parent α_0 phase disappeared at the aging time between 5 min and 10 min, as can be seen from the extinction of the 200 α_0 peak at 10 min. Considering that the hardness curve showed the plateau stage during the process of spinodal decomposition of the α_0 phase after 12 s, it was supposed that the significant amounts of internal strains were introduced in the matrix only at the initial stage of the spinodal decomposition. From the aging time of 10 min to 5,000 min, the hardness increased again to the maximum value even though the increasing rate became very slow from the aging time of 1,000 min. In the XRD pattern until the aging time of about 1,000 min, the metastable α_1' phase which was formed by the spinodal decomposition of the parent α_0 phase was transformed into the stable α_1 phase with the shift of the 111 α_2 peak to the higher angle side. The shift of the 111 α_2 peak with the phase transformation of the metastable α_1' phases into the stable α_1 phase indicates the precipitation of the Ag-rich solute from the Cu-rich matrix. Then, the broad 111 peaks of α_1 and α_2 grew sharp without any change in peak position until the aging time of 20,000 min. As the 111 peak of the α_2 phase grew sharp, the adjacent weak peak of the β phase became obvious, as indicated by an arrow in the XRD pattern at 20,000 min. From the above, it was thought that the first and the second hardening stages were related to the

early stage of spinodal decomposition of the α_0 phase and the formation of the stable α_1 phase from the metastable α_1' phase, respectively. Also, from the sharpening of the XRD peaks, that is, the decrease in FWHM (full width half maximum) during the softening, some microstructural changes which released the internal strains were supposed.

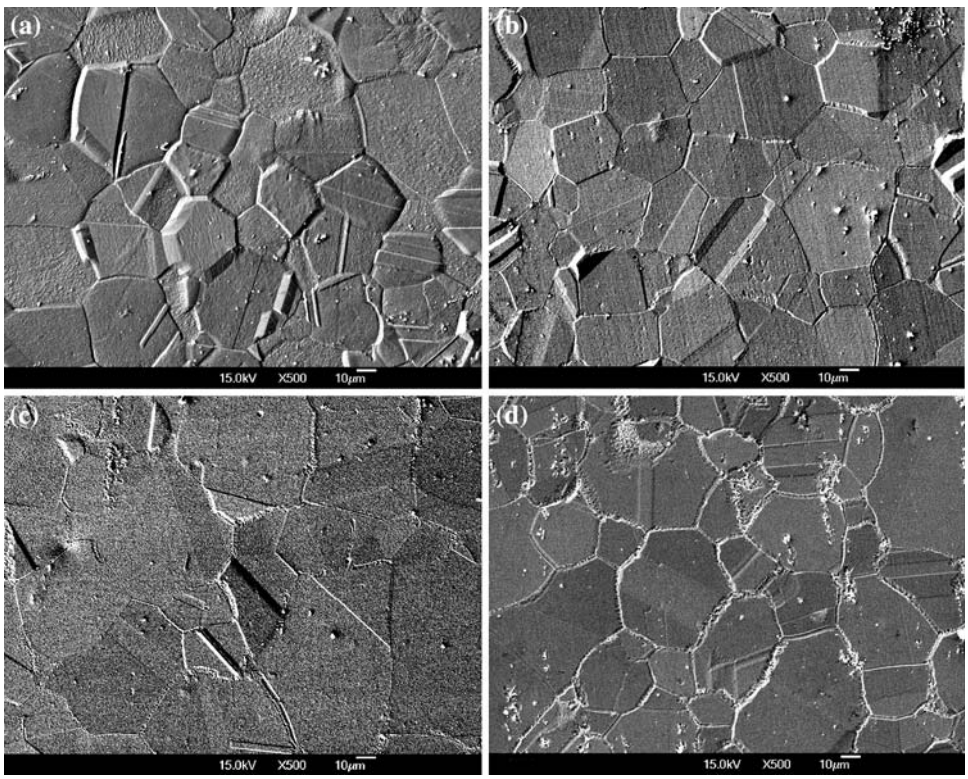

Fig. 3 FESEM photographs of the specimens solution-treated at 750 °C for 10 min (**a**) and aged at 400 °C for 100 (**b**), 5,000 (**c**) and 20,000 min (**d**)

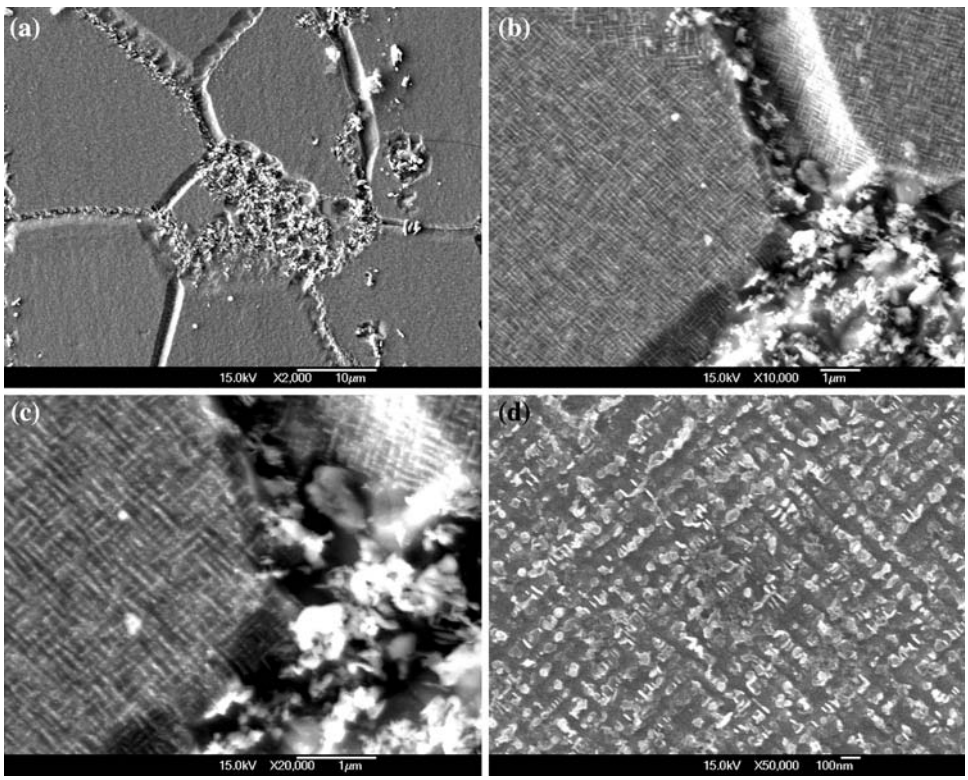

Fig. 4 FESEM photographs at a magnification of 2,000X (**a**), 10,000X (**b**), 20,000X (**c**), and 50,000X (**d**) for the specimen aged at 400 °C for 20,000 min

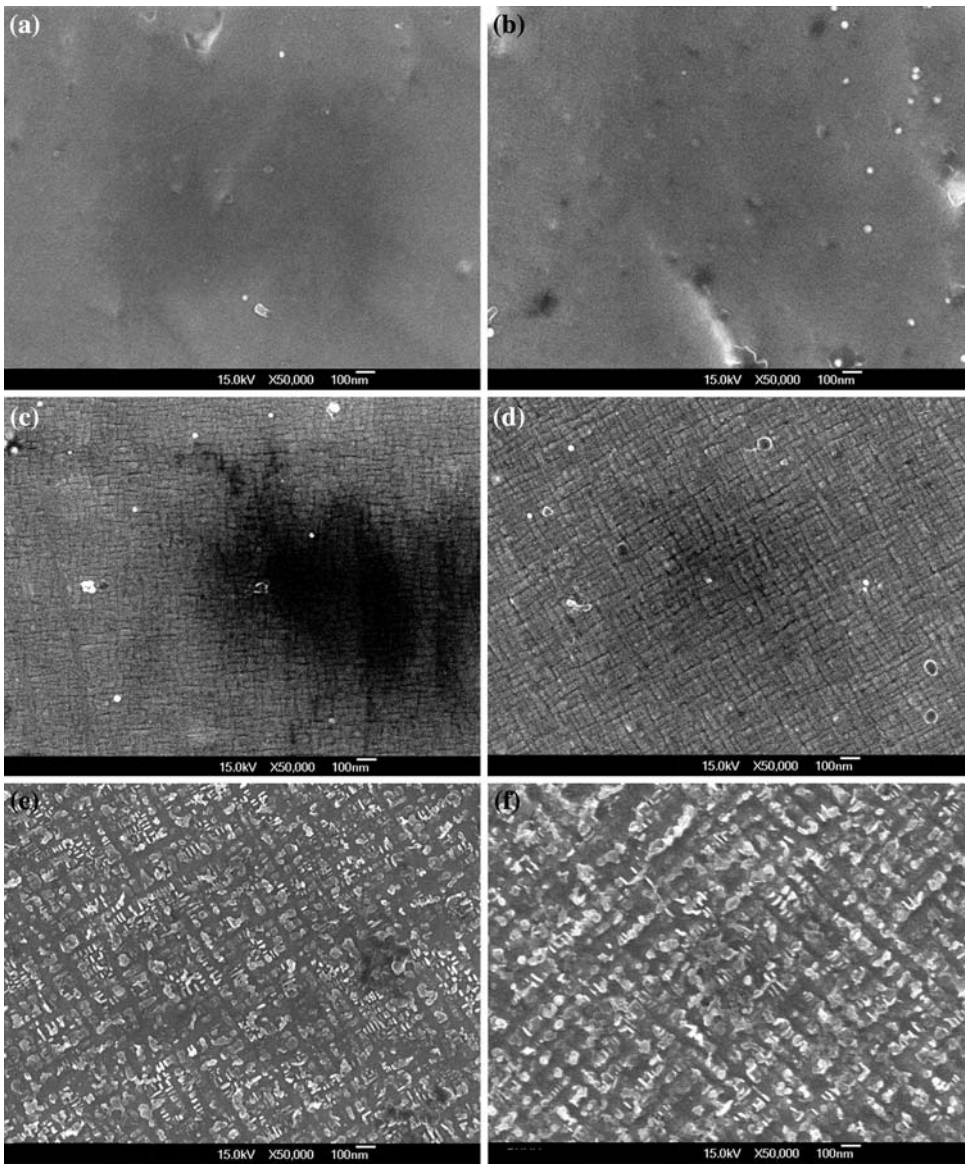

Fig. 5 FESEM photographs at a magnification of 500X for the specimen aged at 400 °C for 2 (**a**), 5 (**b**), 20 (**c**), 100 (**d**), 5,000 (**e**), and 20,000 min (**f**)

Microstructural changes

To investigate the microstructural changes which are related to the hardness changes, FESEM observations were done. Figure 3 shows the FESEM photographs at a magnification of 500X for the specimens solution-treated at 750 °C for 10 min (a) and aged at 400 °C for 100 (b), 5,000 (c), and 20,000 min (d). In the solution-treated specimen (Fig. 3a), an equiaxed structure was observed. In the specimen of increased hardness by aging at 400 °C for 100 min (Fig. 3b), the changes in the grain interior and boundary were not appreciable. In the specimen of maximum hardness by aging at 400 °C for 5,000 min (Fig. 3c), the very fine precipitates in the grain boundary were formed as small amounts. In the overaged specimen by aging at 400 °C for 20,000 min (Fig. 3d), the very fine precipitates in the grain boundary increased a little but did not develop into the grain interior unlike most of the dental alloys in overaged stage [8, 9, 13]. To appreciate the changes in the grain interior, the overaged specimen was magnified up to nano scale. Figure 4 shows the FESEM photographs at a magnification of 2,000X (a), 10,000X (b), 20,000X (c), and 50,000X (d) for the specimen aged at 400 °C for 20,000 min. Besides the grain boundary precipitates, the tweed-like structure which is usually induced by the spinodal decomposition was observed throughout the grain interior [2–5, 14]. In Fig. 4d, the tweed-like structure seemed to be more like a particle chain with a cross hatched structure.

To compare the changes in the grain interior during the aging process, the FESEM photographs at a magnification of 50,000X were obtained for each specimen. Figure 5

shows the FESEM photographs at a magnification of 50,000X for the specimen aged at 400 °C for 2 (a), 5 (b), 20 (c), 100 (d), 5,000 (e), and 20,000 min (f). In Fig. 5a, b which corresponds to the spinodal decomposition period of the parent α_0 phase, the structure in the grain interior did not show an apparent change. In Fig. 5c, a fine closely interlocked block-like structure formed faintly, which became coarse and distinct by further aging until 100 min (Fig. 5d). The corresponding XRD pattern revealed that such a block-like structure formation resulted from the phase transformation of the metastable Ag-rich α_1' phase into the stable Ag-rich α_1 phase with the depletion of Ag from the Cu-rich α_2 phase. In Fig. 5e, the close interlock in the block-like structure became apparently loose. Furthermore, the block-like shape was transformed into the particle-like shape. Considering the XRD pattern of Fig. 2, it is clear that the particle-like precipitates are composed of the stable Ag-rich α_1 phase surrounded by the Cu-rich α_2 matrix. In the overaged specimen of Fig. 5f, the particle-like structure became coarse and chained. Considering the decrease in hardness after the aging time of 5,000 min, it is clear that such a structural change after 5,000 min released the internal strains by reducing the interface between the Ag-rich precipitates and the Cu-rich matrix.

From the above, the first hardening stage in the specimen alloy occurred during the early stage of spinodal decomposition even though the structural change was not detected as it was beyond the resolution of the FESEM . It was thought that the fast hardness increase in the first hardening stage was due to the interaction of dislocation with solute-rich fluctuations which was induced in the early stage of spinodal decomposition. The second hardening stage after the plateau was caused by the formation of the fine block-like structure with high coherency induced by the spinodal decomposition. The softening by overaging was caused by the progress of coarsening and resultant chaining of the Ag-rich α_1 precipitates in the Cu-rich α_2 matrix. The coarsening in the specimen alloy, however, was remarkably delayed due to the uniform fine scale of the structure resulting from the spinodal decomposition. Such stability to coarsening is one of the desirable features for dental alloys.

Element distribution

In order to examine the changes in the element distribution during the aging process, EDS analysis was done for the solution-treated and overaged specimens. Figure 6 shows the FESEM photographs for the specimens solution-treated at 750 °C for 10 min (A) and aged at 400 °C for 20,000 min (B). Element distribution in the area marked by an arrow was analyzed with EDS of FESEM, and the result

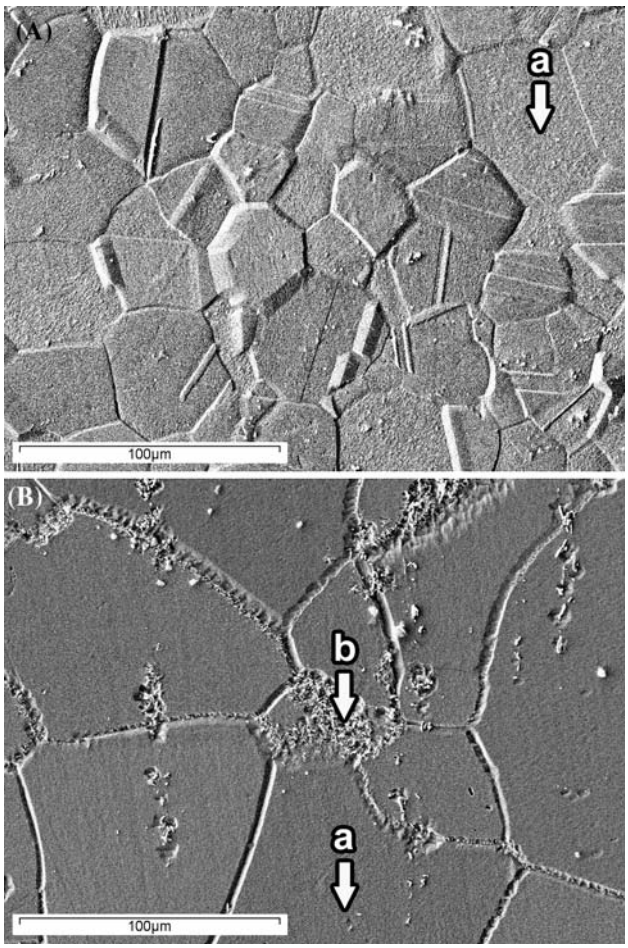

Fig. 6 FESEM photographs for the specimens solution-treated at 750 °C for 10 min (**A**) and aged at 400 °C for 20,000 min (**B**)

is shown in Table 2. In the grain interior of the solution-treated specimen (Fig. 6A-a), the content of each element did not show a remarkable change from that of the alloy composition. In the grain interior of the overaged specimen (Fig. 6B-a), the changes of element distribution by the two-phase decomposition were not detected due to the finer scale. In the grain boundary (Fig. 6B-b), the elements distribution was apparently changed. In the EDS result (Table 2) for the grain boundary of the overaged specimen (Fig. 6B-b), the Zn and Pd content increased apparently, and the Au, Ag, and Cu content decreased compared to those in the matrix of the solution-treated specimen. This

Table 2 EDS analysis for the specimens solution-treated at 750 °C for 30 min (A) and aged at 400 °C for 20,000 min (B) at the regions marked in Fig. 6

Region (at%)	Au	Ag	Cu	Zn	Pd	Pt	Ir
A-a	35.08	21.05	34.77	6.14	2.96	0	0
B-a	36.00	21.18	32.81	6.85	3.16	0	0
B-b	29.24	15.83	27.21	18.47	8.67	0.58	0

indicates that the grain boundary precipitates are mainly composed of the Zn–Pd-rich β phase. Such grain boundary precipitates composed of Pd and extra ingredients of low melting temperature such as Zn and In are frequently observed in dental gold alloys during aging process.

Conclusions

Age-hardening behaviour of a spinodally decomposed low-carat gold alloy composed of 55.0 wt% Au–19.9 wt% Ag–17.0 wt% Cu–4.0 wt% Zn–3.0 wt% Pd–1.0 wt% Pt–0.1 wt% Ir was investigated, and the following results were obtained.

1. An apparent hardness increase occurred at the initial stage of the aging process without incubation periods. Then, after a plateau, the hardness increased to the maximum value, and finally, the softening by overaging occurred.
2. By aging the solution-treated specimen, the parent fcc α_0 phase was transformed into the Ag-rich α_1, Cu-rich α_2, and Zn–Pd-rich β phases through the spinodal decomposition process and the metastable phase formation.
3. The first hardening stage which occurred during the early stage of spinodal decomposition without an apparent structural change was thought to be due to the interaction of dislocation with solute-rich fluctuations.
4. The second hardening stage after the plateau was caused by the formation of the fine block-like structure with high coherency induced by the spinodal decomposition, which corresponded to the phase transformation of the metastable Ag-rich α_1' phase into the stable Ag-rich α_1 phase.
5. The remarkably delayed softening was caused by the slow progress of coarsening and resultant chaining of the Ag-rich α_1 precipitates in the Cu-rich α_2 matrix due to the uniform fine scale of the structure.

References

1. ADA (1972) Guide to dental materials and devices, 6th edn. American Dental Association, Chicago, p 183
2. Yasuda K, Ohta M (1982) J Dent Res 61:473
3. Ohta M, Shiraishi T, Yamane M, Yasuda K (1983) Dent Mater J 2:10
4. Nakagawa M, Yasuda K (1988) J Mater Sci 23:2975
5. Udoh K, Fujiyama H, Hisatsune K, Hasaka M, Yasuda K (1992) J Mater Sci 27:504
6. Kim HI, Jang MI, Jean BJ (1997) J Mater Sci Mater Med 8:333
7. Hamasaki K, Hisatsune K, Udoh K, Tanaka Y, Iijima Y, Takagi O (1998) J Mater Sci Mater Med 9:213
8. Kim HI, Park YH, Lee HK, Seol HJ, Shiraishi T, Hisatsune K (2003) Dent Mater J 22:10
9. Lee JH, Yi SJ, Seol HJ, Kwon YH, Lee JB, Kim HI (2006) J Alloys Compd 425:210
10. Pan LG, Wang JN (2007) J Mater Sci Mater Med 18:171
11. Cullity BD (1978) Elements of X-ray diffraction, 2nd edn. Addison-Wesley publishing Co, Inc, Massachusetts, p 506
12. Massalski TB (1990) Binary alloy phase diagrams, 2nd edn. ASM International, Materials Park, pp 12–13, 28–29, 358–362
13. Kim HI, Jang MI, Kim MS (1999) J Oral Rehabil 26:215
14. Tanaka Y, Udoh K, Hisatsune K, Yasuda K (1994) Philos Mag A 69:925